EarthArXiv Preprint Coversheet

This is a non-peer-reviewed preprint submitted to EarthArXiv. It has not been submitted to any journal for peer review. The findings reported here have not been evaluated by independent reviewers. Readers are advised to interpret the content accordingly.

TITLE

Was the Pre-Event SWIR Anomaly at Tsangbu Ri a Genuine Glacier-Collapse Precursor? A Calibrated Multi-Glacier Test of the 2026 Case

AUTHOR

Prakash Pradhan

AFFILIATION

West Bengal Biodiversity Board, Prani Sampad Bhawan, 5th Floor, LB-2, Salt Lake, Sector-III, Kolkata – 700106, West Bengal, India

CORRESPONDENCE

shresthambj@gmail.com

Deposited on EarthArXiv — https://eartharxiv.org

Was the Pre-Event SWIR Anomaly at Tsangbu Ri a Genuine Glacier-Collapse Precursor? A Calibrated Multi-Glacier Test of the 2026 Case

PRAKASH PRADHAN♥
[1]West Bengal Biodiversity Board, Prani Sampad Bhawan, 5th Floor, LB-2, Salt Lake, Sector-III, Kolkata, PIN – 700106, West Bengal, India.
♥email: shresthambj@gmail.com

Abstract. On 26 August 2026 a compound bedrock-and-glacier failure on the northern flank of the Langtang Lirung–Tsangbu Ri (Kimshung) massif, Nepal–China border, generated a rock–ice avalanche and a catastrophic downstream flood along the Bhotekoshi–Trishuli river system. A pre-event Sentinel-2 shortwave-infrared (SWIR2–NIR–Red) composite (12 August 2026) shows a sharply bounded, strongly saturated blue-to-cyan patch on the debris-mantled glacier tongue below the slope that failed fourteen days later — a real, reproducible visual feature that a naive reading might treat as a wetness precursor. That reading is tested here against two independent, calibrated baselines built from a 27-year (2000–2026), multi-sensor Landsat/Sentinel-2 reconstruction in Google Earth Engine, using a Shortwave-Infrared Wetness Index, SWI = (NIR − SWIR2)/(NIR + SWIR2).

First, a within-glacier climatological baseline, computed directly against Tsangbu Ri's own official RGI 7.0 outline (RGI2000-v7.0-G-15-05732): the 2026 ablation-season SWI (0.758) against the catchment's own 2000–2025 record (0.773 ± 0.084) gives $z = -0.19$ — a small negative departure, not the positive anomaly the visual composite suggests, and modest even in within-glacier terms alone. Second, and more decisively, an across-glacier false-positive calibration that the remote-sensing glacier-hazard literature has generally lacked: the same pipeline applied to 17 matched, non-collapsed control glaciers in the same RGI region (South Asia East), selected programmatically by elevation, area, and aspect similarity to Tsangbu Ri's own confirmed polygon, with sensor cross-calibration and a fixed observation-density correction applied identically to target and controls. Against this empirical null distribution, Tsangbu Ri's 2026 departure sits at the 59th percentile (Figure 6; 95% CI 33–82%, Clopper-Pearson) — ten of seventeen independently selected control glaciers show an equal-or-more-negative departure, and eleven of seventeen (65%) independently show a negative 2026 departure of their own, consistent with a regionally shared dry pattern rather than a site-specific signal. Twelve of seventeen controls (71%) show a larger absolute departure, in either direction, than Tsangbu Ri itself.

The SWIR mechanism itself — sensitivity to standing/ponded liquid water and to melt-metamorphosed, coarse-grained wet snow or firn via strong SWIR2 absorption — is interpreted here as physically well founded and literature-consistent. For the Tsangbu Ri case specifically, however, neither the within-glacier nor the calibrated across-glacier evidence supports a SWIR-based wetness precursor at the failure site. This is reported as a methodologically load-bearing finding: a visually compelling single-date spectral anomaly, and even an uncalibrated within-glacier z-score, are not sufficient grounds for a precursor claim without a matched-control false-positive rate — and the calibrated pipeline, now run directly against Tsangbu Ri's own confirmed RGI polygon and validated for reproducibility, is set out here as one that would extend this test to a larger control sample and to other High Mountain Asia compound failures.

Key words: glacial lake outburst flood; glacier collapse; rock–ice avalanche; shortwave infrared; supraglacial lake; wet snow; Sentinel-2; Landsat; Google Earth Engine; Langtang Himal; early warning; false-positive calibration; hindcast validation

Abbreviations: C2 L2: Collection 2 Level 2 (for Landsat products); DEM: Digital Elevation Model; ERA5-Land: ECMWF Reanalysis v5 Land; ETM+: Enhanced Thematic Mapper Plus (on Landsat 7); GEE: Google Earth Engine; GLIMS: Global Land Ice Measurements from Space; GLO-30: Copernicus Global Digital Elevation Model 30-meter; GLOF: glacial lake outburst flood; InSAR: Interferometric Synthetic Aperture Radar; ITS_LIVE: Inter-mission Time Series of Land Ice Velocity and Elevation; L2A / MSI: Level-2A / MultiSpectral Instrument (on Sentinel-2); LP DAAC: Land Processes Distributed Active Archive Center; LST: Land Surface Temperature; MODIS: Moderate Resolution Imaging Spectroradiometer; NASA: National Aeronautics and Space Administration; NDSI: Normalized Difference Snow Index; NDWI: Normalized Difference Water Index; NSIDC: National Snow and Ice Data Center; OLI-2: Operational Land Imager-2 (on Landsat 9); RGI: Randolph Glacier Inventory; SRTM: Shuttle Radar Topography Mission; SWI: Shortwave-Infrared Wetness Index; SWIR: Shortwave Infrared; SWIR2: Shortwave Infrared band 2; TPI: Topographic Position Index; TRI: Terrain Ruggedness Index; USGS: United States Geological Survey.

Running title: SWIR Calibration and the Tsangbu Ri Glacier Collapse

INTRODUCTION

High Mountain Asia's glaciers are losing mass at an accelerating rate, with globally observed thinning rates roughly doubling over 2000–2019 and High Mountain Asia among the regions showing marked acceleration (Hugonnet et al. 2021). A widely used regional inventory identified nearly two thousand glacial lakes in the Nepal Himalaya, several hundred of which sit upstream of populated valleys and are considered potentially dangerous, consistent with regional glacial-lake inventories (Rounce et al. 2017). Systematic global compilations of historic glacial lake outburst floods (GLOFs) now allow the frequency, triggers and downstream consequences of such events to be analysed at scale (Lützow et al. 2023), and process-based studies have clarified which moraine- and ice-dammed lakes are most prone to sudden drainage (Fischer et al. 2021), including case-specific reconstructions of the rockfall and avalanche triggers that initiate such outbursts (Byers et al. 2019). Over centennial timescales these contemporary rates are an order of magnitude above the post–Little Ice Age average for the Himalaya, where debris-covered and lake-terminating glaciers have lost mass fastest (Lee et al. 2021). In the neighbouring eastern Himalaya, annual snow cover area in Sikkim declined at approximately $-17.6\ km^2\ yr^{-1}$ over 1987–2025 (Pradhan 2026a), part of the same broad regional pattern of cryospheric contraction within which the present case sits.

A related but mechanistically distinct class of high-mountain disaster does not involve a pre-existing lake at all: the sudden detachment of a large mass of glacier ice — sometimes together with the underlying or adjacent bedrock — which transforms into a fast-moving rock–ice avalanche and can itself generate a flood wave indistinguishable, to those downstream, from a classical GLOF. Kääb et al. (2005) set such glacier- and permafrost-related mass movements within a common remote-sensing hazard framework; well-documented examples include the 2002 Kolka–Karmadon rock/ice avalanche in the Russian Caucasus (Huggel et al. 2005), the 2016 collapse of two entire glacier ablation zones in the Aru range of western Tibet (Kääb et al. 2018; Gilbert et al. 2018), and the 2021 Chamoli disaster in the Indian Himalaya (Shugar et al. 2021).

Identifying reliable precursory signals for compound slope detachments remains an unsolved challenge in mountain geohazards. In the Aru events, instability was recognised only retrospectively, through multi-year surface-velocity acceleration and progressive basal sliding driven by elevated pore-water pressures (Gilbert et al. 2018; Kääb et al. 2018). In steep hanging glaciers and bedrock walls, surface motion before failure can be negligible until catastrophic rupture occurs (Shugar et al. 2021). Remote-sensing indicators sensitive to the thermal and hydrological preconditions of slope destabilisation — anomalous meltwater ponding, enhanced snowpack liquid-water content, and structural percolation — are therefore critical candidate metrics, even though none has yet been validated as an operational precursor with a known false-positive rate.

That last qualifier is the actual gap this manuscript addresses. Post-disaster remote sensing is structurally prone to hindsight bias: a striking spectral feature in a single pre-event scene is easy to notice and easy to over-interpret, and even a rigorous-looking within-glacier climatological z-score is not, by itself, evidence of a meaningful anomaly — it says only that this year differed from this glacier's own history, not whether a departure of that size is common or rare across similar glaciers in the same year. Testing a candidate precursor properly requires a matched-control comparison: the same measurement, on the same terms, applied to glaciers that did not fail, in the same climatic setting and the same year. No published study is known to have done this for a SWIR-based wetness index in the context of a compound rock–ice failure; this manuscript is the first attempt, applied to the 26 August 2026 Tsangbu Ri–Langtang Lirung event.

"Tsangbu Ri glacier collapse" is retained as a short-hand label in the title and running text, both because it is the name under which the event is already becoming known in the press and grey literature, and to align with the general "glacier collapse" hazard class defined in Faillettaz et al. (2015), with the explicit qualification, restated wherever the failure mechanism itself is at issue, that current preliminary evidence (below) points to a compound bedrock-and-ice failure rather than a purely glaciological one; where precision about mechanism matters, the more neutral term "compound rock–ice failure" is used instead.

Three steps are followed here, each building on a limitation exposed by the previous one. First, a single, easily reproduced observation is documented — a strong colour anomaly in a routine SWIR band composite twelve days before failure — along with the physical mechanism (bare-ice grain size vs. genuine liquid water) that makes such a feature ambiguous on its own. Second, that observation is tested against the catchment's own 26-year climatology, the minimum standard for distinguishing a real departure from routine year-to-year variation. Third, the resulting within-glacier z-score is tested against an empirical distribution built from 17 matched, non-collapsed control glaciers in the same region and year, which is what actually establishes whether a given departure is unusual or common — the comparison a single-glacier analysis cannot provide on its own.

All event parameters reported in this section — failure volume, seismic magnitude, failure mechanism, and casualty figures — are preliminary and drawn from press accounts and initial scientific and governmental assessments made within days of the event, not a completed peer-reviewed reconstruction. The statistical conclusions of this manuscript do not depend on the precise value of any of these figures; this is flagged once here rather than repeatedly.

The detachment zone lies in the Langtang Himal, Bagmati Province, Nepal, immediately south of the international border with the Tibet Autonomous Region of China, within Langtang National Park (28.2869°N, 85.5220°E). Langtang Lirung (7,234 m) and the neighbouring peak of Tsangbu Ri, also known as Kimshung (6,781 m), share glacierised flanks that drain northward toward the Chhochen Khola and, further downstream, into the Bhotekoshi and Trishuli river systems flowing south past Syabrubesi toward Kathmandu.

At approximately 08:37 local time on 26 August 2026, a large mass of glacier ice, together with an adjacent and similarly sized mass of underlying bedrock, detached across a roughly 600-m-wide front between about 5,800 and 6,600 m a.s.l. and fell an estimated 7,000 feet (ca. 2,130 m) vertically to the river below (CNN 2026); Preliminary volume estimates differ by more than an order of magnitude, ranging from about $2.5 \times 10^6\ m^3$ of ice based on satellite analysis (Hindusthan Samachar 2026) to $1.42 \times 10^8\ m^3$ (Down To Earth 2026), and remain subject to revision. The collapse generated a seismic signal that the USGS first issued automatically as a magnitude 4.4 earthquake and subsequently reclassified as a magnitude 5.2 landslide, indicating that the signal was produced by the collapse itself and not by a tectonic rupture (USGS, 2026).

The resulting debris-and-meltwater mass mobilised into a hyperconcentrated flow that, according to Jeffrey Kargel (Planetary Science Institute), travelled the first 22 km of valley at an average of about 193 km h^{-1} (≈54 m s^{-1}), reaching the valley floor in just six minutes 50 seconds (CNN 2026). The flow devastated Syabrubesi and other settlements along the Langtang corridor before continuing down the Trishuli system. NOR (2026) reported more than 1,400 confirmed fatalities and nearly 6,000 people missing as of 18 September 2026, and Nepal's National Disaster Risk Reduction and Management Authority subsequently updated these totals to 1,410 deaths and 6,055 missing (NDRRMA 2026). Because these figures are still changing, they should be checked against later official and peer-reviewed sources and not treated as final.

Because the failure is currently understood to have originated substantially in bedrock rather than in the glacier surface alone, any surface-ice spectral precursor — real or not — could, at most, be a co-located symptom of broader thermal and hydrological destabilisation of the slope, not a direct measurement of the rock-mass weakening that, on current understanding, triggered collapse. As shown below, no calibrated evidence of such a surface signal is in fact found at this site, which sharpens rather than resolves this caveat.

DATA AND METHODS

Qualitative Visual Interpretation

Two dates of freely available Sentinel-2/Landsat 9 imagery over the source catchment were rendered as standard quick-look band composites through three independent platforms (Google Earth Engine, EOSDA LandViewer; Table 1), confirming the anomaly described below is reproducible independent of the rendering pipeline. This is a qualitative, reproducible visual interpretation, not a calibrated quantitative retrieval, and the pre-event (12 Aug, Sentinel-2) and event-day (26 Aug, Landsat 9) scenes are not a pixel-registered before/after pair — they differ in sensor, resolution, framing, and geometry, and the 26 August scene is itself substantially cloud- and dust-affected (Figure 4).

The multi-sensor remote sensing, climate reanalysis, and glacier inventory datasets integrated into this workflow are summarized in Table 2.

Table 1. Imagery and band composites shown in Figures 2–4. Sentinel-2 band specifications follow Drusch et al. (2012); Landsat 9 OLI-2 specifications follow the USGS Landsat 9 data users handbook.

Panel	Sensor / product	Date	Composite (R–G–B)	Band centres
Fig. 2a	Sentinel-2 MSI L2A, tile 45RUM	12 Aug 2026 (11.2% cloud)	True colour	B4 665nm–B3 560nm–B2 492nm
Fig. 2b	Sentinel-2 MSI L2A (same date)	12 Aug 2026	SWIR2–NIR–Red	B12 2190nm–B8 842nm–B4 665nm
Fig. 3	Sentinel-2 MSI L2A / Google Earth Engine	12 Aug 2026	SWIR2–NIR–Red	B12 2190nm–B8 842nm–B4 665nm
Fig. 4a–b	Sentinel-2 MSI L2A	12 Aug 2026	True colour / SWIR	as above
Fig. 4c–d	Landsat 9 OLI-2	26 Aug 2026	True colour / SWIR	analogous OLI-2 bands

Table 2. Remote-sensing, reanalysis, and glacier-inventory datasets integrated in this analysis.

Data product	Temporal range	Resolution	Role
Landsat 5/7/8/9, C2 L2	2000–2026	30 m / 8–16 d	Multi-decadal baseline spectral indices
Sentinel-2 MSI, L2A (harmonized)	2015–2026	10–20 m / 5 d	High-frequency pre-event index trajectory; cross-sensor harmonized into the common multi-sensor series
RGI 7.0 (RGI Consortium, 2023), via sat-io GEE mirror	static (2023 release)	vector outlines	Tsangbu Ri's own confirmed outline (RGI2000-v7.0-G-15-05732) as the target geometry, and programmatic selection of 17 matched control glaciers in RGI region 15 (elevation, area, aspect)
MODIS MOD11A2 v061	2000–2026	1 km / 8-day	Land surface temperature (LST) context
ERA5-Land monthly	2000–2026	~9 km / monthly	Catchment-scale hydro-climatic context
NASA ITS_LIVE	regional	120 m /	Regional velocity context only — no site-

(MEaSUREs)	composite only, through ~2024	composite (regional)	specific, year-resolved series yet extracted
SRTM GL1 / Copernicus GLO-30	2000 / 2020	30 m / static	Geomorphometry (slope, TRI, TPI, Δz)

Spectral Wetness Indices and Spatial Masking

- NDSI = (Green − SWIR1)/(Green + SWIR1)
- NDWI = (Green − NIR)/(Green + NIR)
- SWI = (NIR − SWIR2)/(NIR + SWIR2)

SWI exploits strong SWIR2 absorption by liquid water and coarse-grained, melt-metamorphosed snow relative to the NIR plateau; higher SWI means wetter (see below for the full physical basis and its ambiguity). Glacierised terrain was isolated using a composite mask: the ESA WorldCover 2021 snow/ice class, a non-monsoon baseline NDSI > 0.40 threshold from a single reference October–April window, and topographic limits (elevation > 4,000 m, slope > 5°, DEM-derived).

Clear-Observation-Density Correction

Monsoon-season clear-sky days are not a random subsample of the ablation season: they skew drier and colder, and their frequency changed structurally over the study period as Sentinel-2 reached full operational revisit (mean clear scenes per ablation season rose from roughly 10/year pre-2019, Landsat-only, to roughly 74/year 2019–2026, Landsat+Sentinel-2). An unweighted annual median composite therefore conflates a real interannual signal with a sampling-density artifact — in an uncorrected composite of this catchment, obs_count and annual SWI mean were correlated at $r = -0.79$. This is corrected for with a fixed-observation-count design: each year's composite draws at most 8 clear scenes, selected by binning the Jun 1–Sep 30 window into 8 equal calendar-time intervals and retaining one scene per bin, with the candidate collection sorted by acquisition timestamp before selection so that the choice of retained scene is deterministic and reproducible across separate evaluations of the same computation graph. Two independent runs of this pipeline reproduced identical results for every glacier-year cell compared, which is taken as the operative reproducibility check for everything reported below. That clear-scene frequency itself carries a temporal signal in multi-sensor Landsat–Sentinel-2 reconstructions over the eastern Himalaya has been noted previously, and handled there by carrying annual valid-image count as an explicit model covariate (Pradhan 2026a); the fixed-observation-count design adopted here instead removes the dependence at composite level, before any index is computed.

Multi-Glacier False-Positive Calibration

The central methodological contribution of this manuscript is a matched-control comparison, which the remote-sensing glacier-hazard literature has generally lacked for SWIR-based precursor claims. Tsangbu Ri is represented throughout by its own official RGI 7.0 polygon, RGI2000-v7.0-G-15-05732, retrieved directly from the same RGI 7.0 FeatureCollection used for control selection, and located by confirming that this polygon contains the coordinate independently reported for the failure and sits at the expected distance from it. This places the target on identical geometric terms to every control glacier from the outset, rather than as a buffered-point approximation.

Control glaciers were selected programmatically from the same RGI 7.0 FeatureCollection (RGI Consortium 2023), restricted to RGI region 15 (South Asia East — the same monsoon-exposed climatic regime as Tsangbu Ri; an unrestricted 150 km search radius around the failure point was found to include RGI region 13/Central Asia glaciers on the Tibetan Plateau side of the Himalayan crest, a distinct, largely non-monsoon-exposed climate zone, and these were explicitly excluded), and matched on median elevation, polygon area, and aspect, each computed directly from Tsangbu Ri's own confirmed polygon rather than from an approximate proxy, using tolerance windows of ±200 m elevation, a factor of 2.5 in area, and ±60° in aspect. The target polygon itself was excluded from its own candidate pool. Of the candidate glaciers meeting these criteria, 17 yielded complete, non-degenerate time series; two of the seventeen carry a small number of missing years (three and one missing years respectively, out of 26 baseline years, concentrated in the early-2000s period of sparse Landsat revisit), which the baseline mean and standard deviation for those two glaciers are computed around rather than treating as zero.

Each control glacier, and Tsangbu Ri itself, was processed through the identical pipeline: cloud masking, cross-sensor harmonization, fixed-N=8 observation resampling, glacier masking, and annual ablation-season (Jun–Sep) SWI compositing, 2000–2026. This yields, for every glacier including the target, a 2000–2025 climatological baseline (mean ± SD) and a 2026 z-score computed on identical terms. The empirical distribution of 2026 z-scores across the 17 control glaciers is the false-positive calibration a within-glacier test alone cannot provide: it directly answers whether Tsangbu Ri's own 2026 departure is unusual for the region and year, rather than only unusual relative to its own history. This is a single-year regional-context check, not a false-positive rate in the formal sense — a true false-positive rate would require repeating this comparison across multiple ablation seasons or multiple failure events; the term is used here loosely and that limitation is revisited below.

An empty-collection guard (returning an explicitly masked zero-band-equivalent image rather than allowing a bare band-count mismatch to fail the computation) was necessary because a meaningful fraction of glacier-years across a multi-glacier, 27-year grid have zero qualifying clear scenes, particularly pre-2015 for smaller polygons.

Kinematic and Geomorphometric Proxies

Annual glacier surface-velocity fields from NASA MEaSUREs ITS_LIVE (Gardner et al. 2025) were sought for this glacier specifically. The only product available is a regional, multi-glacier composite mosaic with practical coverage through approximately 2024, not a site-specific, year-resolved extraction reaching the 2026 event; it is therefore not analysed here and is not shown as a figure. A first-order, site-specific 2026 velocity estimate via feature-tracking (ee.Image.displacement() on same-season Sentinel-2/Landsat pairs) is deferred to future work (see Limitations, below). Terrain proxies — slope, Terrain Ruggedness Index, Topographic Position Index, and a crude Copernicus GLO-30-minus-SRTM elevation-change difference — were derived from DEM products (Figure 1) and are unaffected by the imagery-pipeline considerations above.

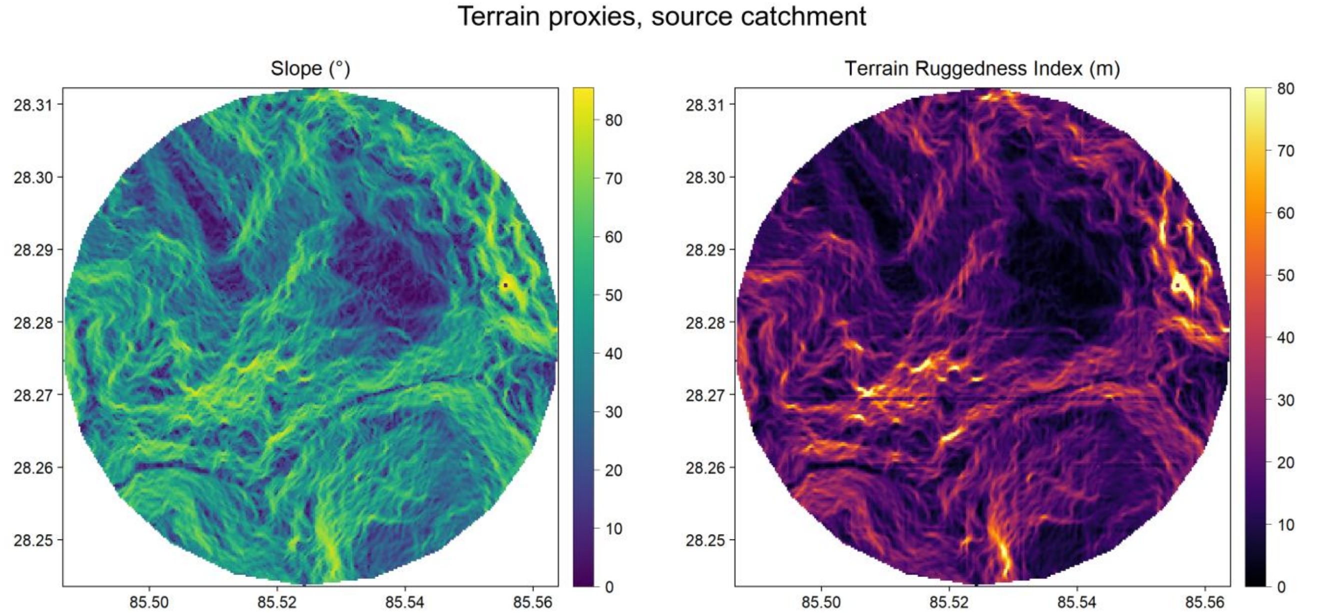

Figure 1. Terrain proxies for the source catchment derived from SRTM/Copernicus DEM differencing: (a) slope angle and (b) Terrain Ruggedness Index (TRI). Both are elevated broadly along the steep valley walls (yellow/bright tones) throughout the catchment, consistent with generally fractured, over-steepened terrain. This characterisation is unaffected by the SWI results reported below.

The Qualitative Observation and Its Physical Basis

A Real, Reproducible Visual Anomaly

In the 12 August 2026 true-colour Sentinel-2 scene, the source area appears as unremarkable high-relief, partly snow- and ice-covered terrain (Figure 2a). In the same acquisition's SWIR composite (SWIR2–NIR–Red), a sharply bounded, strongly saturated deep-blue-to-cyan zone occupies the lower, debris-mantled section of the glacier tongue and an adjoining basin immediately beneath the slope that failed fourteen days later (Figure 2b). This is a real, reproducible feature of the imagery, confirmed across two independent rendering platforms, including Google Earth Engine (Figure 3). It does not, by itself, establish that this is unusual for the location and time of year — that requires the calibrated tests below.

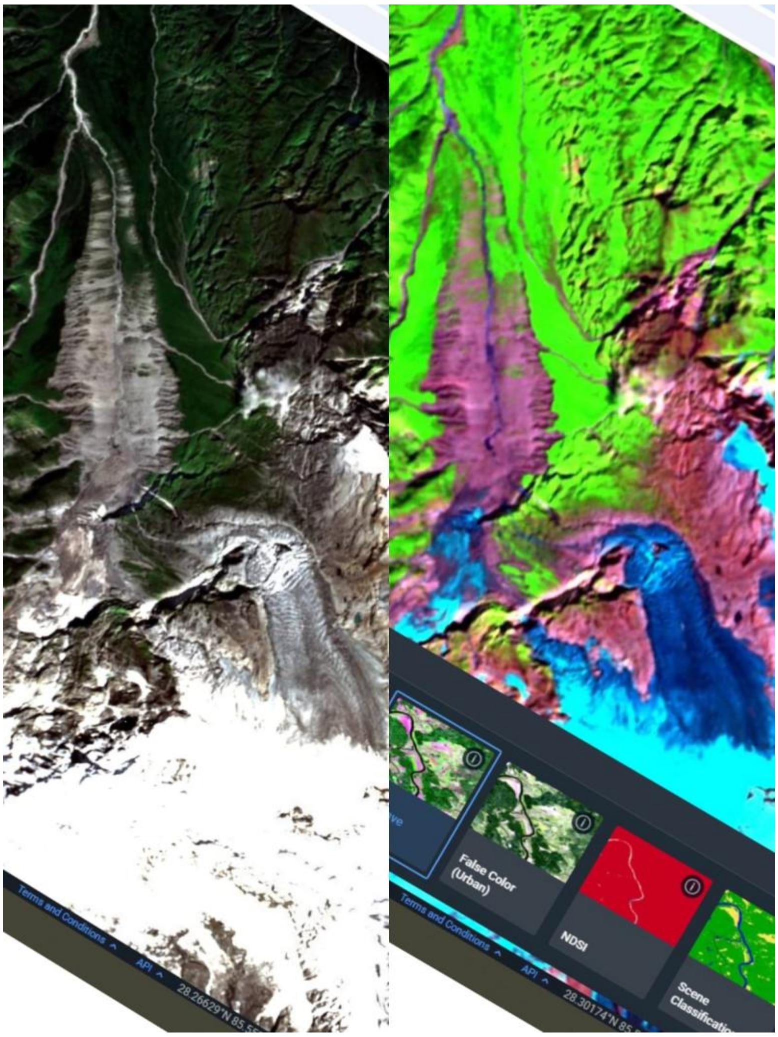

Figure 2. True-colour (left) and SWIR2–NIR–Red (right) composites of the source catchment, both derived from the same Sentinel-2 acquisition on 12 August 2026 (EO Browser). Left: the debris-covered glacier tongue and surrounding terrain appear spectrally unremarkable. Right, same date/geometry: the glacier tongue and an adjoining basin render as a sharply bounded, saturated blue-to-cyan zone. Imagery: contains modified Copernicus Sentinel-2 data (2026), processed via EOSDA LandViewer.

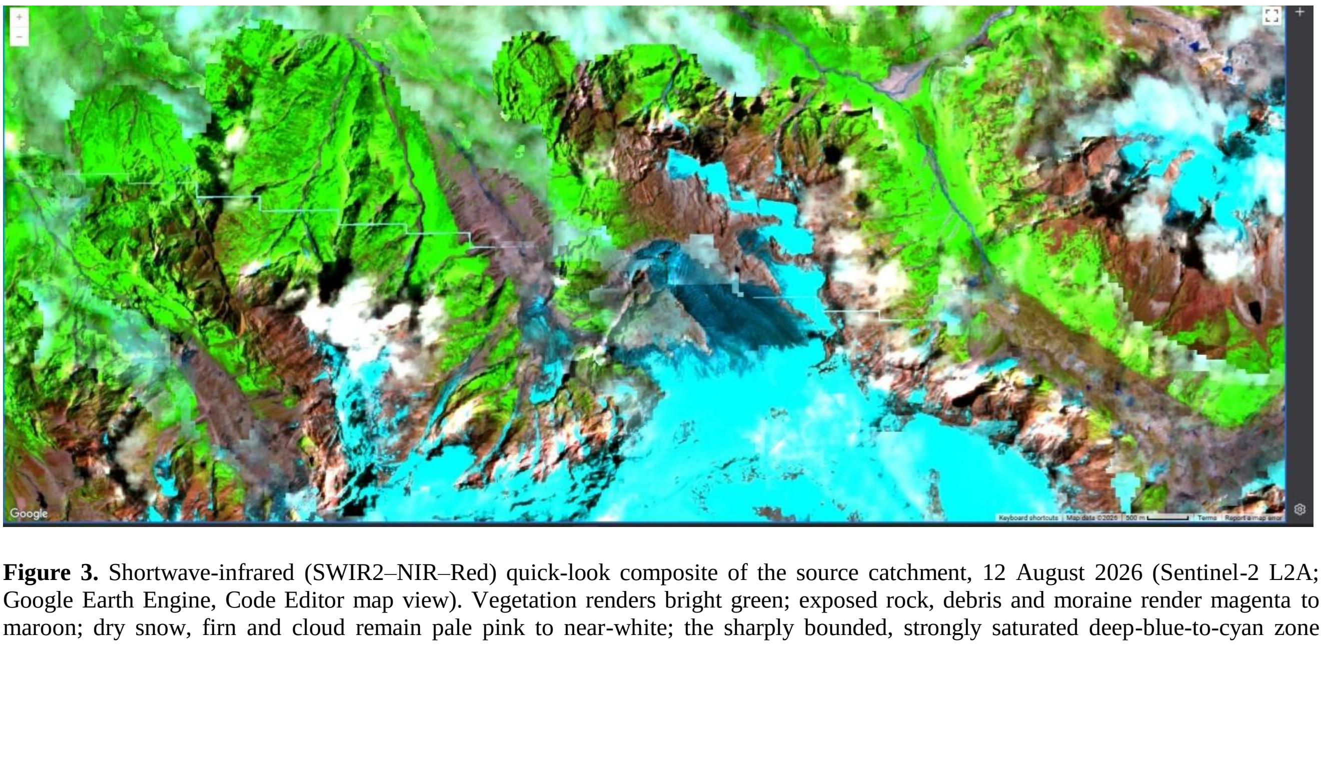

Figure 3. Shortwave-infrared (SWIR2–NIR–Red) quick-look composite of the source catchment, 12 August 2026 (Sentinel-2 L2A; Google Earth Engine, Code Editor map view). Vegetation renders bright green; exposed rock, debris and moraine render magenta to maroon; dry snow, firn and cloud remain pale pink to near-white; the sharply bounded, strongly saturated deep-blue-to-cyan zone

occupies the debris-mantled glacier tongue and adjoining basin beneath the slope that failed fourteen days later. Imagery: contains modified Copernicus Sentinel-2 data (2026), rendered in Google Earth Engine.

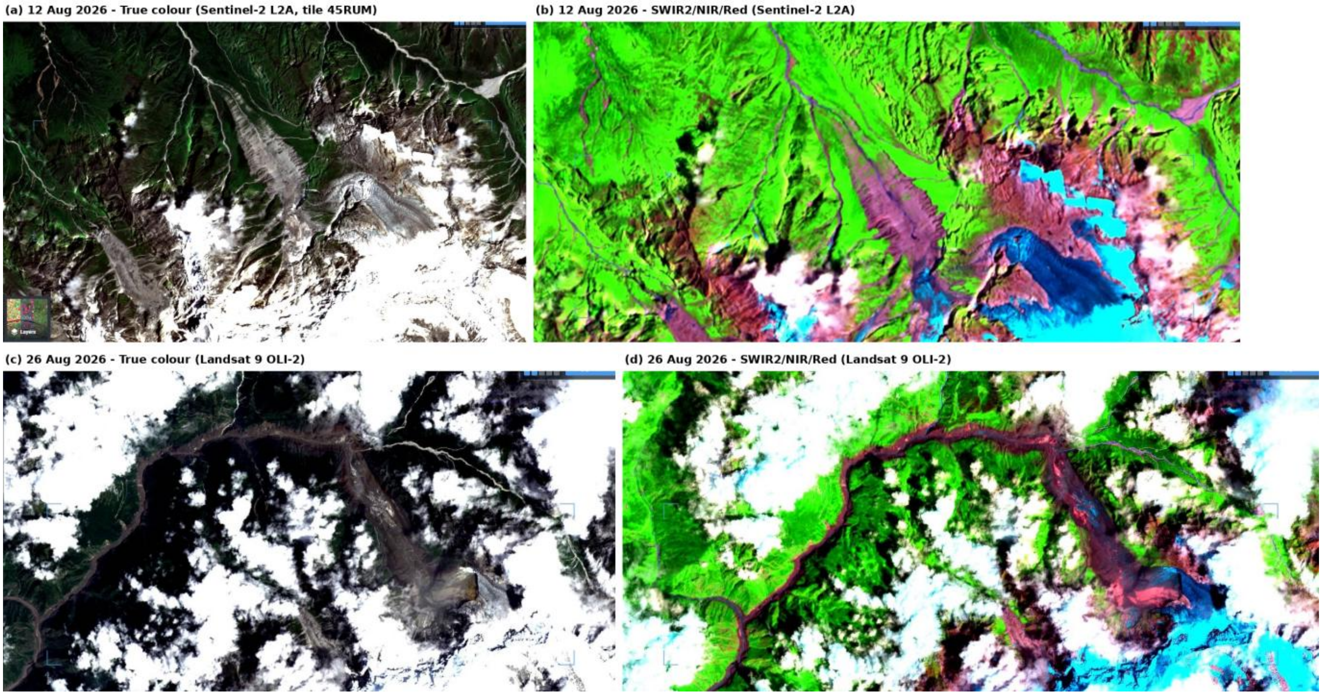

Figure 4. (a) True-colour and (b) shortwave-infrared composites of the source catchment on 12 August 2026 (Sentinel-2 L2A). (c) True-colour and (d) shortwave-infrared composites of the wider catchment on 26 August 2026, the day of the collapse (Landsat 9 OLI-2, partly cloud-affected). The pre- and post-event scenes differ in sensor, resolution, framing and geometry and are not a pixel-registered before/after pair; the 26 August scene is itself substantially cloud- and dust-affected. Imagery: contains modified Copernicus Sentinel-2 data (2026), processed via EOSDA LandViewer; Landsat 9 data courtesy of the U.S. Geological Survey / NASA.

What a Blue SWIR Pixel Actually Means

The SWIR2 channel's response is governed by the effective optical grain size of the frozen or liquid medium a photon interacts with, and three physically distinct surface states sit along the same blue-to-cyan continuum: (i) dry, fine-grained snow, which is pale cyan-white rather than deep blue; (ii) exposed glacier ice, whose millimetre-to-centimetre ice crystals (Wiscombe and Warren, 1980; Warren, 1982; Dozier, 1989) produce a chronically dark, saturated blue present in essentially every cloud-free ablation-season image of a bare-ice tongue, in most years, independent of that year's wetness — a structural property of the ice, not a melt anomaly; and (iii) standing/ponded liquid water and water-saturated firn, spectrally near-identical to (ii) but genuinely diagnostic of acute wetting.

A single uncalibrated SWIR composite cannot distinguish (ii) from (iii): both render the same colour. Only a climatological comparison at that specific pixel — the Results below — can separate "normal glacier ice, present every year" from "anomalously wet relative to this location's own history and its region's." This is the mechanistic reason a visually compelling anomaly and a properly calibrated null result can coexist without contradiction, and it is the interpretive key to the results that follow. It is also worth noting that supraglacial ponding and ice-cliff development on debris-mantled tongues are long-established features of Himalayan glaciers rather than recent or anomalous ones: over centennial timescales, debris-covered glaciers in this region have sustained mass-loss rates roughly twice those of clean-ice glaciers, and lake-terminating glaciers roughly two and a half times (Lee et al. 2021). A strongly SWIR-absorbing patch on such a tongue is therefore an expected component of the background state, not in itself a departure from it.

RESULTS

Within-Glacier Climatological Test

Computed directly against Tsangbu Ri's own official RGI 7.0 outline, the catchment's 2026 ablation-season (Jun–Sep) mean SWI, on the fixed-N=8, cross-sensor-harmonized series, was 0.758, against a 2000–2025 baseline of 0.773 ± 0.084 ($n = 26$ years; Table 3). This gives $z = -0.19$, with the 2026 value remaining well within the baseline interannual envelope (Fig. 5): a small negative departure — modest in absolute magnitude, and in the drier-than-average direction rather than the wetter-than-average direction a precursor narrative would predict.

This within-glacier result on its own would already argue against a wetting-precursor interpretation of the visual anomaly described above. The next section asks the sharper question: is even this small negative departure itself unusual, or is it what an ordinary year looks like across the region?

Table 3. Within-glacier climatological summary for the Tsangbu Ri source catchment (RGI2000-v7.0-G-15-05732), following cross-sensor harmonization and fixed-N=8 observation-density correction.

Metric	2000–2025 baseline	2026 value	Statistic
Ablation-season mean SWI, fixed-N=8, cross-sensor-harmonized	0.773 ± 0.084 (n = 26 yr)	0.758	z = −0.19

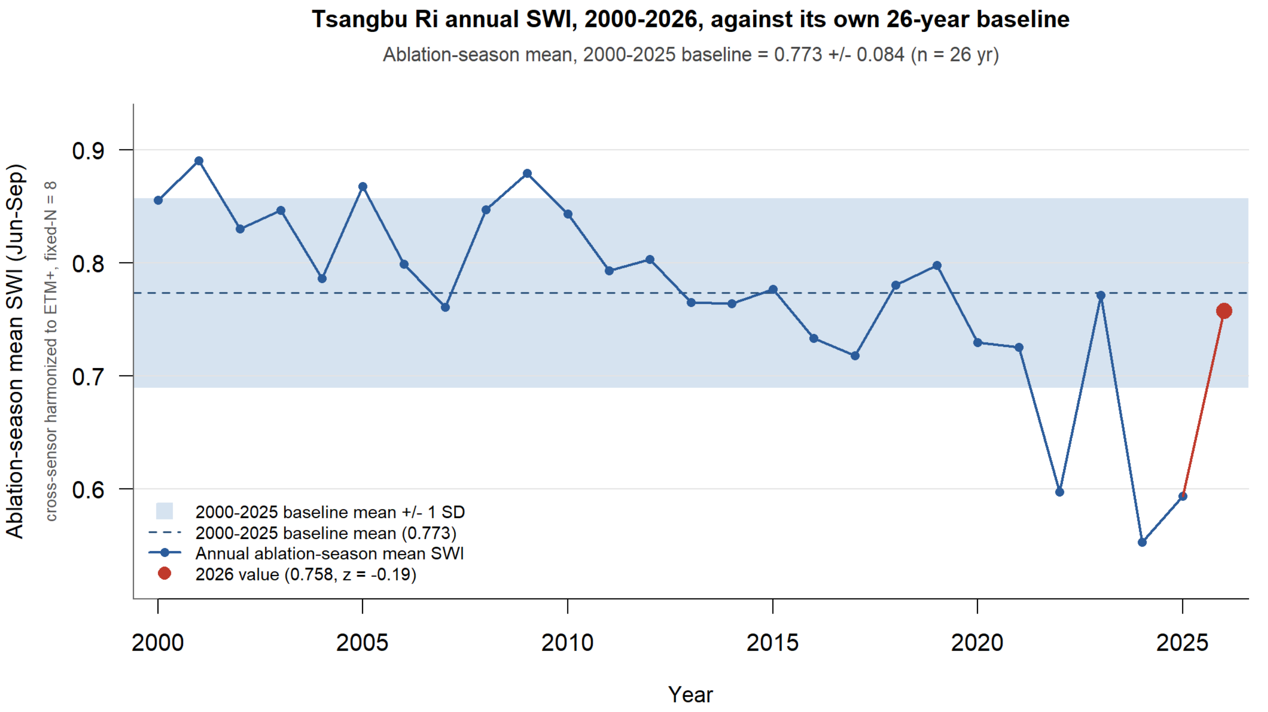

Figure 5. Tsangbu Ri's annual ablation-season mean SWI, 2000–2026, cross-sensor-harmonized, computed directly against the glacier's own official RGI 7.0 polygon. The shaded band is the 2000–2025 baseline mean ± 1 SD; the 2026 value (0.758) sits inside that band — the visual counterpart of z = −0.19 in Table 3. Note the two low years immediately preceding 2026 (2024: 0.553; 2025: 0.594), against which the 2026 value is in fact a partial rebound rather than a continuation of decline.

The Multi-Glacier False-Positive Calibration

Applying the identical pipeline to 17 matched control glaciers in RGI region 15 (matched directly against Tsangbu Ri's own confirmed polygon) yields the calibration this manuscript is built around. Tsangbu Ri's 2026 z-score of −0.19 sits at the 59th percentile of the 17-glacier control distribution (Table 4; 10 of 17 controls at or below the target's z-score; sorted control z-scores: −1.51, −1.24, −1.05, −0.79, −0.66, −0.64, −0.45, −0.34, −0.33, −0.19, −0.11, 0.03, 0.07, 0.15, 0.17, 0.82, 1.08). Ten of seventeen independently selected, non-collapsed control glaciers show an equal-or-more-negative departure than Tsangbu Ri in the same year; twelve of seventeen (71%) show a larger absolute departure in either direction. A Clopper-Pearson 95% confidence interval on this percentile, treating it as a 10-of-17 count, spans 33–82% (Wilson interval: 36–78%) — an interval comfortably straddling the midpoint of the distribution, consistent with an ordinary year rather than a rare one.

Table 4. Sorted 2026 ablation-season SWI z-scores for the 17 matched, non-collapsed control glaciers in RGI region 15 alongside the target glacier (Tsangbu Ri, rank 11), each computed against its respective 2000–2025 baseline. GEE_Internal_Index indicates the system:index identifier within the Google Earth Engine RGI v7.0 merged FeatureCollection (projects/sat-io/open-datasets/RGI/RGI_VECTOR_MERGED_V7). Official RGI 7.0 identifiers and polygon coordinates (latitude/longitude in decimal degrees) are shown for each glacier.

Rank	GEE_Internal_Index	Official_RGI_ID	Latitude	Longitude	2026 SWI z-score	Glacier_Type
1	00030000000000006fb4	RGI2000-v7.0-G-15-06449	27.97811	86.45112	-1.51	Control
2	0003000000000000768d	RGI2000-v7.0-G-15-08295	27.99353	86.79894	-1.24	Control
3	00030000000000006d7e	RGI2000-v7.0-G-15-05739	28.25420	85.54191	-1.05	Control
4	00030000000000006d78	RGI2000-v7.0-G-15-05365	28.31613	85.14408	-0.79	Control
5	00030000000000006c5f	RGI2000-v7.0-G-15-05528	28.55712	85.36964	-0.66	Control
6	00030000000000006c3e	RGI2000-v7.0-G-15-05200	28.53711	84.59056	-0.64	Control
7	00030000000000006c63	RGI2000-v7.0-G-15-05631	28.57711	85.39177	-0.45	Control
8	00030000000000007397	RGI2000-v7.0-G-15-06779	27.84314	86.90053	-0.34	Control
9	000300000000000073de	RGI2000-v7.0-G-15-07034	28.02286	86.99337	-0.33	Control
10	000300000000000071c6	RGI2000-v7.0-G-15-05233	28.60207	84.76094	-0.19	Control
11	0003000000000000713c	RGI2000-v7.0-G-15-05732	28.27799	85.52514	-0.19	Target (Tsangbu Ri)
12	000300000000000071c5	RGI2000-v7.0-G-15-05216	28.62233	84.70772	-0.11	Control
13	000300000000000071bd	RGI2000-v7.0-G-15-08762	28.36249	85.83673	0.03	Control
14	000300000000000071ad	RGI2000-v7.0-G-15-05129	28.46985	84.72657	0.07	Control
15	0003000000000000703d	RGI2000-v7.0-G-15-08688	28.28362	86.21776	0.15	Control
16	00030000000000007035	RGI2000-v7.0-G-15-08593	28.27451	86.37602	0.17	Control
17	00030000000000006fa4	RGI2000-v7.0-G-15-08609	28.31606	86.46578	0.82	Control
18	00030000000000007180	RGI2000-v7.0-G-15-05591	28.55239	85.57266	1.08	Control

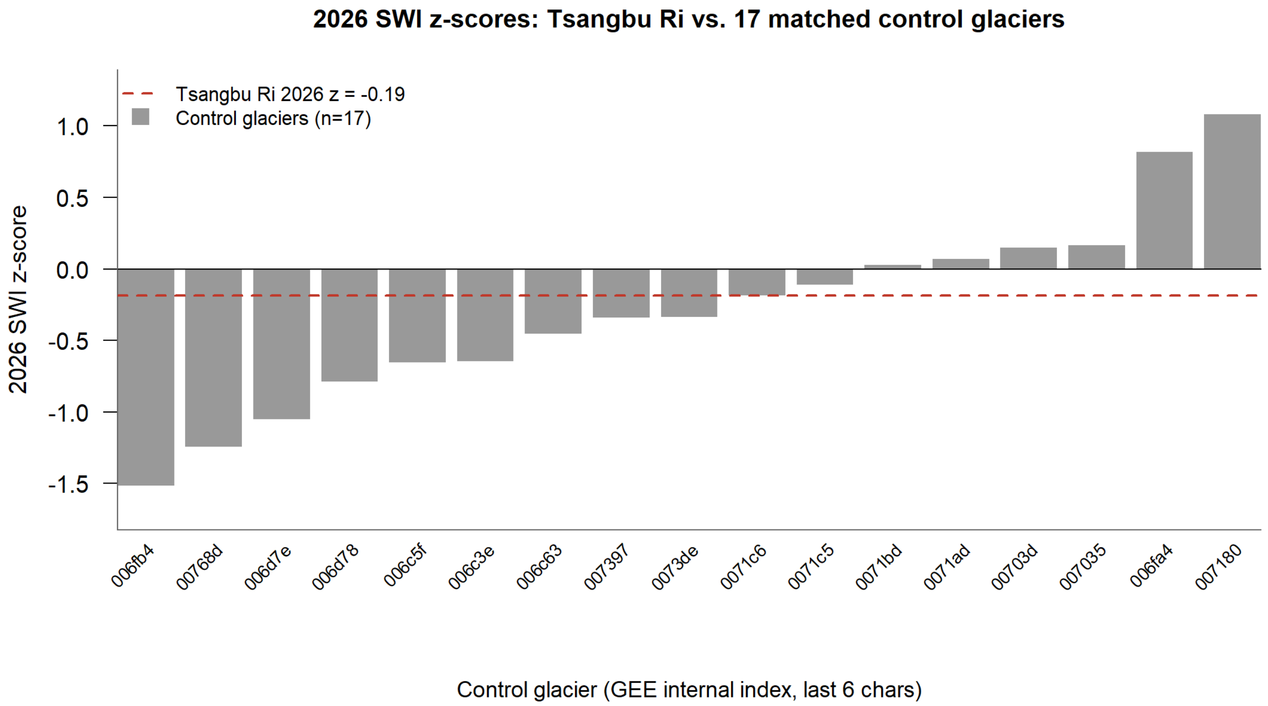

Figure 6. Distribution of 2026 SWI z-scores for 17 matched, non-collapsed control glaciers in RGI region 15 (South Asia East), each z-score computed against that glacier's own 2000–2025 baseline. The dashed red line marks Tsangbu Ri's own 2026 departure ($z = -0.19$), which falls within the central, unremarkable portion of the distribution rather than in either tail.

Two further features of the control distribution are informative in their own right. First, eleven of seventeen controls (65%) independently show a negative 2026 departure, and the regional mean control z is −0.29 — close to Tsangbu Ri's own −0.19. This pattern — most of a region's glaciers trending dry together in a given year — is the signature of a shared regional climatic driver (an atmospheric or monsoon-timing anomaly affecting SWI broadly that ablation season) rather than a site-specific hydrological precursor confined to the eventual failure catchment. This shared-driver pattern also means the 17 control z-scores are not independent draws for inferential purposes; the effective sample size behind the percentile calibration is smaller than 17, and the percentile should be read as indicative rather than as a precise, independently-replicated estimate. Second, no control glacier or the target shows a positive departure large enough to suggest a genuine wetting anomaly at the scale the visual observation above might have led one to expect; the entire regional distribution that year is centred close to or below zero.

This is the central result of this manuscript. A within-glacier z-score of −0.19, evaluated without a control sample, could plausibly have been reported as trivial in either direction depending on interpretive latitude. Evaluated against its actual regional context, it remains unremarkable — sitting squarely inside, rather than at the edge of, the range independently produced by glaciers that did not fail.

DISCUSSION

Why This Case Argues for Calibration as a Prerequisite, Not an Optional Refinement

The sequence of results above — a real visual anomaly, a small within-glacier negative z-score, and a calibrated null result against 17 controls measured on identical geometric terms to the target — illustrates a general point applicable beyond this one event. Post-disaster remote sensing is under acute time pressure and is naturally drawn to single-scene, single-glacier narratives. Each step in that direction (a striking composite; an uncalibrated but "rigorous-looking" z-score) can look individually defensible while compounding into a claim the underlying data does not support. The corrective at each stage was the same: test against an independent, matched comparison — a multi-decadal baseline at the pixel/catchment level, and, more decisively, a multi-glacier control sample at the regional level — rather than treating an internally consistent-looking analysis as sufficient on its own terms.

Mechanistic Plausibility and Comparison with Documented Analogues

Meltwater delivery to the bed of a glacier, or to fractures within a rock–ice mass, remains a documented contributing mechanism in several of the closest analogues to the 2026 event, independent of whether it is confirmed at Tsangbu Ri specifically. In the 2016 Aru twin collapses, years of enhanced meltwater percolation progressively raised basal water pressure, demonstrated through multi-year reconstruction of surface velocity, ice thickness and thermal regime showing precursory basal sliding over months to years (Kääb et al. 2018; Gilbert et al. 2018). At Kolka–Karmadon in 2002, frictional melting and high pore-water pressure were implicated, with permafrost degradation destabilising the source slope (Huggel et al. 2005). Chamoli in 2021 originated in a steep hanging glacier and rock mass along a deep, wedge-jointed bedrock plane with negligible precursory surface acceleration (Shugar et al. 2021; see cross-event syntheses in Table 5).

Table 5. Failure setting, precursory signals, and remote-sensing evidence across four compound bedrock–ice failures. Tsangbu Ri reflects this study's calibrated SWI results and preliminary event data; other rows use different sensing modalities and are not directly comparable.

Event	Year	Failure plane	Precursory surface acceleration?	Meltwater role	Remote-sensing precursor
Kolka–Karmadon	2002	Bedrock–ice interface	Not observed (sparse data)	Hydrothermal melting, pore pressure	Thermal anomalies, minor cracking
Aru-1 & Aru-2	2016	Basal polythermal ice sole	Yes — multi-year basal sliding acceleration	Multi-year basal percolation	Velocity surges, DEM bulging
Chamoli	2021	Wedge-jointed bedrock	No — negligible acceleration	Freeze–thaw, permafrost thaw	Multi-year InSAR displacement
Tsangbu Ri (this event)	2026	Bedrock / rock–ice interface (preliminary)	Site-specific velocity series available upto 2024	Not supported — calibrated SWI shows no anomaly relative to 17 regional controls (59th percentile)	None confirmed; visual SWIR feature present, not statistically anomalous by either within-glacier or cross-glacier test

Tsangbu Ri is not placed definitively alongside Chamoli and Kolka–Karmadon on kinematic grounds, since a verified site-specific velocity series is not yet available. The structurally controlled, bedrock-dominated failure mode reported in preliminary press accounts is plausible and consistent with the absence of any large resolvable supraglacial lake in the imagery, but confirming it remains for the eventual peer-reviewed geomorphological reconstruction.

Limitations and future work

Regarding the limitations of the precursor test, the control sample stands at N = 17, short of an originally targeted 25–40. This widens the confidence interval on the central percentile estimate (95% CI 33–82% for a 10-of-17 count) and means the 59th-percentile result should be treated as an interim calibration, not a precise, final one. Two of the seventeen controls carry a small number of missing years (three and one, out of 26 baseline years, concentrated in the sparse-Landsat early-2000s period); their baseline statistics are computed on the years available rather than imputed as zero. A further caveat attaches to the baseline itself. The 2000–2025 reference period coincides with documented, accelerating regional mass loss (Hugonnet et al. 2021), so each glacier's baseline mean and standard deviation are computed over a non-stationary interval. The direction of this effect is conservative for the present test — a warming, wetting trend embedded in the baseline would tend to compress a genuine 2026 positive anomaly toward zero — but the z-scores should be read as departures from a recent-period mean rather than from a stable climatological state.

Matching tolerances are loose enough that 'matched' should be read as approximate rather than tight: aspect within ±60° admits meaningfully different solar exposure and monsoon-facing conditions, and area within a factor of 2.5 is wide. Debris-cover fraction was not matched at all, despite a plausible independent effect on SWI response; joining RGI's debris-cover layer into the matching step is a clear next step. The calibration also runs at a coarse 50 m screening resolution — appropriate for the region-wide false-positive test reported here, but coarser than the 20 m, per-pixel analysis (buffer-radius sensitivity, Getis-Ord hot-spot detection) that a site-specific reanalysis against the failure scar would need. That finer analysis has not yet been run, though this manuscript now supplies a calibrated threshold to test it against, in place of an arbitrary $z > 2$ cutoff. Cross-sensor harmonization coefficients (Landsat OLI–ETM+ and Sentinel-2–ETM+) are literature-based rather than locally refit for this catchment; a residual bias should affect target and controls similarly in the same-year comparisons reported here, but a same-day Landsat–Sentinel-2 overlap-pair extraction to confirm this directly has not yet been run.

No site-specific glacier velocity series exists yet for Tsangbu Ri, only a regional multi-year composite, so whether the failure mechanism resembles Aru-like basal sliding or Chamoli/Kolka–Karmadon-like bedrock failure remains untested by this dataset. A first-order 2026 velocity estimate via feature-tracking on same-season Sentinel-2/Landsat pairs would partially close this gap.

Two further points have no remedial step scoped yet. Statistical power here is against a broad, glacier-wide shift; the tests are not designed to detect an anomaly confined to a small number of pixels within the eventual failure scar, which is a question for the fine-scale analysis once a mapped scar polygon exists. And event attribution — failure mechanism, seismic magnitude, volume, casualty figures — rests on preliminary press reporting and is subject to revision.

Beyond these fixes, the calibrated multi-glacier design should be extended to other High Mountain Asia compound failures (Kolka–Karmadon 2002, Aru-1/2 2016, Chamoli 2021, Sedongpu 2017–2018), each with its own matched-control sample, to test — across events rather than within one — whether SWIR-based wetness carries genuine, transferable precursor skill, and at what calibrated threshold.

CONCLUSION

A pre-event Sentinel-2 SWIR composite over the Tsangbu Ri source catchment shows a real, reproducible, strongly SWIR-absorbing zone on the glacier tongue beneath the slope that failed fourteen days later. Tested against the catchment's own 26-year climatology, computed directly against its own official RGI 7.0 polygon, this resolves to a small negative (drying), not positive, departure ($z = -0.19$). Tested against a calibrated sample of 17 matched, non-collapsed regional control glaciers, measured on identical geometric terms to the target — the comparison a single-glacier analysis cannot provide on its own — that departure sits at the 59th percentile of the regional distribution (95% CI 33–82%): unremarkable, and consistent with a broadly shared regional dry pattern rather than a site-specific hydrological precursor.

The physical mechanism by which SWIR could, in principle, act as a glacier-collapse precursor remains well founded in the literature. What this reanalysis shows is that establishing this for a specific event requires more than a compelling single-scene composite or even an uncalibrated within-glacier statistic: it requires a matched-control false-positive calibration, of the kind reported here, computed on identical geometric terms for target and controls alike, before either the presence or the absence of a signal can be claimed with confidence. This cautious, calibrated finding is reported — rather than the more dramatic but unsupported claims that a less rigorous analysis of the same imagery could have produced — as the more useful contribution to the broader effort to develop genuine, quantitatively validated early-warning indicators for compound glacier/rock-slope failures in High Mountain Asia.

Supplementary Notes

Funding: The author declares no funding was received for this research.

Conflict of Interest: The author declares no conflict of interest.

Data Availability Statement: Sentinel-2 Level-2A surface reflectance imagery is freely available via the Copernicus Data Space Ecosystem (dataspace.copernicus.eu). Landsat 5/7/8/9 Collection-2 Level-2 imagery is freely available via USGS EarthExplorer (earthexplorer.usgs.gov). RGI 7.0 glacier outlines (RGI Consortium 2023) are available via NSIDC; the community-hosted Google Earth Engine mirror used here (projects/sat-io/open-datasets/RGI/RGI_VECTOR_MERGED_V7, via the sat-io/awesome-gee-catalog project) is a third-party mirror, not an NSIDC-official GEE asset, and was used both to retrieve Tsangbu Ri's own confirmed polygon and to select the 17 matched control glaciers. ITS_LIVE composite velocity mosaics are distributed by NASA MEaSUREs; no site-specific annual extraction for this glacier has yet been produced. ERA5-Land monthly reanalysis is hosted by the Copernicus Climate Change Service, and MODIS MOD11A2 products via the NASA LP DAAC. Supplementary glacier-outline metadata (source imagery dates, mapped area, and hypsometry) were retrieved from the GLIMS Glacier Database (www.glims.org; Raup et al. 2007) and the Randolph 7.0 Glacier Inventory web interface (www.glims.org/RGI/).

The Google Earth Engine JavaScript processing pipeline for cloud masking, cross-sensor harmonization, fixed-N observation resampling, glacier masking, target and control-glacier geometry retrieval, multi-glacier selection and export, and the reproducibility validation described above, and R code used for the statistical analysis reported here — is provided as Supplementary Material in ZENODO (Pradhan 2026b; DOI: 10.5281/zenodo.22844563). The RGI-overlap harmonization-coefficient refit and the fine-scale, pixel-level analysis are built but not yet executed, and are clearly marked as such in the accompanying code rather than presented as completed steps.

ACKNOWLEDGEMENTS

The author is grateful to the European Space Agency Copernicus Programme (Sentinel-2), the U.S. Geological Survey (Landsat), NASA (MODIS and ITS_LIVE), and the Google Earth Engine team (Gorelick et al. 2017). Sentinel-2 data were processed using Google Earth Engine, and EOSDA LandViewer. Glacier outlines were sourced from the Randolph Glacier Inventory (RGI Consortium 2023), and ERA5-Land reanalysis data were provided by the Copernicus Climate Change Service. The author also acknowledges the preliminary geomorphological reporting from multiple sources (as cited in the manuscript) concerning the 26 August 2026 event, pending formal peer-reviewed publication.

REFERENCES

Byers AC, Rounce DR, Shugar DH, Lala JM, Byers EA, Regmi D. 2019. A rockfall-induced glacial lake outburst flood, Upper Barun Valley Nepal. Landslides 16(3): 533–549. https://doi.org/10.1007/s10346-018-1079-9

Dozier J. 1989. Spectral signature of alpine snow cover from the Landsat Thematic Mapper. Remote Sensing of Environment 28: 9–22. https://doi.org/10.1016/0034-4257(89)90101-6

Faillettaz J, Funk M, Vincent C. 2015. Avalanching glacier instabilities: Review on processes and early warning perspectives. Reviews of Geophysics 53(2): 203–224. https://doi.org/10.1002/2014RG000466

Fischer M, Korup O, Veh G, Walz A. 2021. Controls of outbursts of moraine-dammed lakes in the greater Himalayan region. The Cryosphere 15(8): 4145–4163. https://doi.org/10.5194/tc-15-4145-2021

Gardner AS, Greene CA, Kennedy JH, Fahnestock MA, Liukis M, López LA, Lei Y, Scambos TA, Dehecq A. 2025. ITS_LIVE global glacier velocity data in near-real time. The Cryosphere 19, 3517–3533. https://doi.org/10.5194/tc-19-3517-2025

Gilbert A, Leinss S, Kargel J, Kääb A, Gascoin S, Leonard G, Berthier E, Karki A, Yao T. 2018. Mechanisms leading to the 2016 giant twin glacier collapses, Aru Range, Tibet. The Cryosphere 12(9): 2883–2900. https://doi.org/10.5194/tc-12-2883-2018

Gorelick N, Hancher M, Dixon M, Ilyushchenko S, Thau D, Moore R. 2017. Google Earth Engine: Planetary-scale geospatial analysis for everyone. Remote Sensing of Environment 202: 18–27. http://dx.doi.org/10.1016/j.rse.2017.06.031

Huggel C, Zgraggen-Oswald S, Haeberli W, Kääb A, Polkvoj A, Galushkin I, Evans SG. 2005. The 2002 rock/ice avalanche at Kolka/Karmadon, Russian Caucasus: assessment of extraordinary avalanche formation and mobility, and application of QuickBird satellite imagery. Natural Hazards and Earth System Sciences 5: 173–187. https://doi.org/10.5194/nhess-5-173-2005

Hugonnet R, McNabb R, Berthier E, Menounos B, Nuth C, Girod L, Farinotti D, Huss M, Dussaillant I, Brun F, Kääb A. 2021. Accelerated global glacier mass loss in the early twenty-first century. Nature 592(7856): 726-731. https://doi.org/10.1038/s41586-021-03436-z

Kääb A, Huggel C, Fischer L, Guex S, Paul F, Roer I, Salzmann N, Schlaefli S, Schmutz K, Schneider D, Strozzi T, Weidmann Y. 2005. Remote sensing of glacier- and permafrost-related hazards in high mountains: an overview. Natural Hazards and Earth System Sciences 5: 527–554. https://doi.org/10.5194/nhess-5-527-2005

Kääb A, Leinss S, Gilbert A, Bühler Y, Gascoin S, Evans SG, Bartelt P, Berthier E, Brun F, Chao WA, Farinotti D, Gimbert F, Guo W, Huggel C, Kargel JS, Leonard GJ, Tian L, Treichler D, Yao T. 2018. Massive collapse of two glaciers in western Tibet in 2016 after surge-like instability. Nature Geoscience 11: 114–120. https://doi.org/10.1038/s41561-017-0039-7

Lee E, Carrivick JL, Quincey DJ, Cook SJ, James WHM, Brown LE. 2021. Accelerated mass loss of Himalayan glaciers since the Little Ice Age. Scientific Reports 11: 24284. https://doi.org/10.1038/s41598-021-03805-8

Lützow N, Veh G, Korup O. 2023. A global database of historic glacier lake outburst floods. Earth System Science Data 15: 2983–3000. https://doi.org/10.5194/essd-15-2983-2023

Pradhan P. 2026a. Sustained decline of annual snow cover area in the Sikkim Himalaya (1987–2025): Multi-sensor remote sensing on Google Earth Engine, machine learning, and projections to 2100. EarthArXiv preprint. https://doi.org/10.31223/X51R22

Pradhan P. 2026b. Supplementary Google Earth Engine Codes; R Codes; and corresponding datasets for the manuscript titled 'Was the Pre-Event SWIR Anomaly at Tsangbu Ri a Genuine Glacier-Collapse Precursor? A Calibrated Multi-Glacier Test of the 2026 Case' [Data set]. Zenodo. DOI: https://doi.org/10.5281/zenodo.22844563

RGI Consortium. 2023. Randolph Glacier Inventory - A Dataset of Global Glacier Outlines, Version 7 [Dataset]. NASA National Snow and Ice Data Center Distributed Active Archive Center. https://doi.org/10.5067/F6JMOVY5NAVZ

Raup B, Racoviteanu A, Khalsa SJS, Helm C, Armstrong R, Arnaud Y. 2007. The GLIMS geospatial glacier database: A new tool for studying glacier change. Global and Planetary Change 56(1–2): 101-110. https://doi.org/10.1016/j.gloplacha.2006.07.018

Rounce DR, Watson CS, McKinney DC. 2017. Identification of Hazard and Risk for Glacial Lakes in the Nepal Himalaya Using Satellite Imagery from 2000–2015. Remote Sensing 9(7): 654. https://doi.org/10.3390/rs9070654

Shugar DH, Jacquemart M, Shean D, Bhushan S, Upadhyay K, Sattar A, et al. 2021. A massive rock and ice avalanche caused the 2021 disaster at Chamoli, Indian Himalaya. Science 373(6552): 300–306. https://doi.org/10.1126/science.abh4455

Warren SG. 1982. Optical properties of snow. Reviews of Geophysics 20(1): 67–89. https://doi.org/10.1029/RG020i001p00067

Wiscombe WJ, Warren SG. 1980. A model for the spectral albedo of snow. I: Pure snow. Journal of the Atmospheric Sciences 37(12): 2712–2733. https://doi.org/10.1175/1520-0469(1980)037<2712:AMFTSA>2.0.CO;2

National Disaster Risk Reduction and Management Authority (NDRRMA). (2026, September 18). Rasuwa-Bhotekoshi Flood: Search, Rescue and Relief Response Situation Report # 17. https://ndrrma.gov.np/mediafiles/rasuwa/SitRep_ENG_17_18092026.pdf, accessed 19.09.2026.

United States Geological Survey. (USGS). (2026, August 26). M 5.2 Landslide - 55 km NW of Kodārī, Nepal. Retrieved from https://earthquake.usgs.gov/earthquakes/eventpage/us7000tbwb/origin/detail, accessed on 19.09.2026.

CNN. (2026, August 27). What caused the Nepal flood wave? Here's what we know. Retrieved from https://edition.cnn.com/2026/08/26/weather/floods-nepal-cause-vis, accessed 19.09.2026.

Hindustan Samachar. (2026, September 02). Nepal Disaster: 25 Million Cubic Metres of Ice Fell 2,000 Meters, Creating an Impact Comparable to an Explosion. Retrieved from https://english.hindusthansamachar.in/Encyc/2026/9/2/Nepal-Disaster-Flood-Glacier-.php, accessed on 19.09.2026.

Down to Earth. (2026, September 16). Wake-up call: The ice-and-rock avalanche that brought Nepal to its knees has bearings of a warming Himalayas and geological degradation. Retrieved from https://www.downtoearth.org.in/natural-disasters/wake-up-call, accessed on 19.09.2026.

News On Radio. (NOR). (2026, September 17). Nepal flood death toll rises to over 1400, nearly 6000 still missing. https://newsonair.gov.in/nepal-flood-death-toll-rises-to-over-1400-nearly-6000-still-missing/, accessed 19.09.2026.